Available online at www.sciencedirect.com
ScienceDirect
Dyes and Pigments 76 (2008) 535–541
DYES and PIGMENTS
www.elsevier.com/locate/dyepig

Photocatalytic effects of titania supported nanoporous MCM-41 on degradation of methyl orange in the presence of electron acceptors

Sambandam Anandan*

Department of Chemistry, National Institute of Technology, Trichy 620 015, Tamil Nadu, India

Received 27 July 2006; received in revised form 5 August 2006; accepted 12 September 2006
Available online 19 December 2006

Abstract

This study reports on the synthesis and photocatalytic evaluation of nanometer sized titania supported MCM-41 (TiMCM-41) by photodegrading methyl orange in the presence of electron acceptors such as peroxomonosulphate (PMS), peroxodisulphate (PDS) and H_2O_2 using visible-light irradiation to prove it is a better photocatalyst for advanced oxidation technologies (AOTs). This system is relatively inexpensive, reproducible, extremely stable and efficient in complete degradation of dye in aqueous solution. In order to obtain maximum information about the performance of TiMCM-41 catalyst, we did experiments under different operating conditions, i.e., variation of amount of catalyst, concentration of dye and electron acceptors. In addition to the above, a comparative study on the photocatalytic activities of colloidal TiO_2 was also made.

Keywords: TiMCM-41; MeOr; Electron acceptors; Photocatalytic degradation

1. Introduction

The rapid industrialization, besides its benefit, has resulted in hazardous effects on the environment. For example, effluents from pulp and paper, petrochemical, textile and dyeing industries discharge different types of pollutants that are toxic, carcinogenic, and mutagenic to the aquatic lives as well as human beings. Advanced oxidation technologies (AOTs) are effective remediation and treatment methods due to their ability to completely degrade wide variety of organic pollutants and microbial substances [1–3]. However, the extremely specific molecular selectivity is required for the removal of most important organic pollutants such as 4-nonylphenol in water, an endocrine disrupter from sewage disposal plants, which show their estrogenic activities at very low concentrations and their feminizing effect in fish is a serious problem in terms of ecological system conservation [4–6].

To overcome such problems, in addition to AOTs silica based nanoporous materials were particularly used because they have a great deal of interest in their application in the field of catalysis, sensing, guest–host chemical supporters, molecular transport properties and adsorption due to their high surface areas and large ordered pores ranging from 0.74 to 10 nm [7–15]. Also, the beneficial effect of silica based nanoporous materials, which shows no photoactivity, probably relates to the preferential adsorption of the substrates on silica. Hence, efforts have been made by many researchers to introduce metal ions (Ti, Al, or V) into the nanoporous materials to effectively increase the catalytic activities [16–18]. Among them, TiO_2 supported nanoporous materials are known to be the most effective photocatalysts because they are biologically and chemically inert, and photostable with high band gap energy. In addition, as titanium-containing nanoporous materials have higher active surface areas than pure titania, these materials are expected to have enhanced photocatalytic efficiencies [19–21]. Hence, the present investigation addresses the photodegradation processes of azo dye (methyl orange; MeOr) with TiMCM-41 as a photocatalyst

* Tel.: +91 431 2501801/10x3601; fax: +91 431 2500133.
E-mail addresses: sanand99@yahoo.com, sanand@nitt.edu

0143-7208/$ - see front matter © 2006 Elsevier Ltd. All rights reserved.
doi:10.1016/j.dyepig.2006.09.014

and PMS, PDS and H_2O_2 as electron acceptors by combining the above two processes to get effective outcome in the field of environmental research.

2. Experimental

2.1. Materials and methods

The chemicals used are titanium(IV) isopropoxide, tetraethoxysilane, peroxomonosulphate (Aldrich), trimethyl stearylammonium chloride, peroxodisulphate (Wako Chemicals) and methyl orange (Fluka). All the other chemicals used are the purest research grade available. HPLC grade distilled water (Wako Chemicals) was used in all experiments. Colloidal TiO_2 particles were synthesized by the method reported by Gratzel et al. [22] starting from titanium(IV) isopropoxide in 2-propanol. The diameters of the nanochannels were calculated from the X-ray diffraction data (measured using Rigaku diffractometer, Cu Kα radiation, Japan) and the surface area which was measured by BET method (Flowsorb II 2300 of Micrometrics, Inc.). IR spectra are recorded using a Shimadzu FT-IR 8400 S spectrophotometer by employing KBr pellet technique. Diffused reflectance UV–vis spectra of the samples were recorded using a Shimadzu UV–vis 2550 spectrophotometer. The photoactivity test was conducted under ambient atmospheric conditions in a 50 mL Pyrex glass bottle to prevent absorbing UV light. A 150 W Xenon arc lamp (intensity of incident radiation is 2.443×10^{-9} einsteins/(cm^2 s)) was used as the light source. In order to ensure adsorption equilibrium, the solution was stirred for about 30 min in dark, prior to irradiation. The apparent kinetics of disappearance of the substrate methyl orange was determined by following the concentration of the substance ($\lambda_{max} = 466$ nm) at various time intervals using UV–vis spectrophotometer after a certain period of irradiation of the catalyst suspension and then filtered with a 0.45 μm PVDF filter.

2.2. Preparation of the photocatalyst

Nanometer sized TiMCM-41 (0.020 Ti/Si ratio) was synthesized by the dilute solution routes starting from trimethyl stearylammonium chloride as the micellar component with referring to a procedure described in the literature [23]. About 2.2 g of trimethyl stearylammonium chloride was dissolved in 52 mL of water at 40 °C. Ammonium hydroxide (Aldrich; 28% in H_2O; 26 mL) was then added under stirring. Addition of 10 mL of tetraethoxysilane and 0.03 g of titanium isopropoxide to the solution was followed by continued stirring for 3 h at room temperature. The gel was then transferred to a Teflon-lined autoclave and held at 110 °C for 48 h. Filtration and washing with distilled water gave TiMCM-41. Template removal was typically conducted by heating at 100 °C for 12 h followed by calcination at 550 °C for 5 h. Similarly, MCM-41 is prepared without titanium isopropoxide for comparison.

3. Results and discussion

3.1. Characterization of the photocatalyst

Fig. 1a depicts the XRD profile of the pure MCM-41 and TiMCM-41. The strongest peak which appeared between 1.8 and 10.0°, is indexed as the (100) reflection. The XRD patterns of TiMCM-41 are free from crystalline TiO_2 and suggest that the hexagonal pore order of MCM-41 nanochannels was maintained well after modification also. The *d*-spacing of the TiMCM-41 reduced from 43.7 to 42.8 Å (unmodified MCM-41) as a result of the introduction of titania in MCM-41 nanochannels. XRD peak (Fig. 1b), characteristic of anatase titania was observed around $2\theta = 25°$ for TiMCM-41 sample which also confirms that Ti is in anatase form only in nanochannels [24]. Using the d_{100} value of 42.8 Å and 43.7 Å for TiMCM-41 and MCM-41, the pore diameter of 4.35 nm is obtained for TiMCM-41 (surface area = 861 m^2/g) and 4.56 nm for unmodified MCM-41 (surface area = 1029 m^2/g) sample using Fenelonov et al.'s [25] pore diameter determination procedure.

Infrared analysis of the TiMCM-41 samples confirmed the presence of the finger print bands below 1100 cm^{-1} which are characteristic of asymmetric (1080 cm^{-1}) and symmetric (810 cm^{-1}) stretching vibrations, respectively, of framework Si–O–Si (Fig. 1c). The Si–O–Ti linkage stretching band appears at 970 cm^{-1} for the TiMCM-41 sample. The absence of Ti–O–Ti stretching band at 710 cm^{-1} for TiMCM-41 sample generally infers that no crystalline titanium dioxide in the pore system of MCM-41. But the XRD spectrum of TiMCM-41 does clearly show a reflection peak which is typical for anatase being a crystalline form of TiO_2. Hence explanation for these contradicting results could be that the sensitivity of IR spectroscopy is not sufficient to detect the small amount of Ti–O–Ti bonds besides the large amount of Si–O–Si bonds.

Fig. 1d shows the diffused reflectance spectra of TiMCM-41, the band edge of 360 nm is significantly blue shifted from the band edge of 380–400 nm for bulk TiO_2 semiconductor (anatase form). Attribution of such blue shift is due to the well known quantum size effect for semiconductors as the particle size decreases [26]. Also the colloidal TiO_2 particles exhibit absorption sharply at $\lambda < 400$ nm [22] which agrees well with the 3.2 eV band gap of anatase.

3.2. Factors influencing the decomposition efficiency of the photocatalyst (TiMCM-41) for photodegradation of methyl orange (MeOr)

Heterogeneous photocatalysis appears as an emerging and interesting technology for the degradation of dyes as it can utilize sunlight as a source of energy, which is free and inexhaustible [1–3]. For this, classical photocatalyst (TiO_2) seems to have the most interesting attributes such as high stability, good performance and low cost. This is because, semiconductor TiO_2 generate electrons and holes upon irradiation with light energy. It is broadly accepted that hydroxyl radicals ($OH^{\bullet}$) are produced in water matrices from the direct oxidation of H_2O, OH^- ions or terminal –OH groups present on the

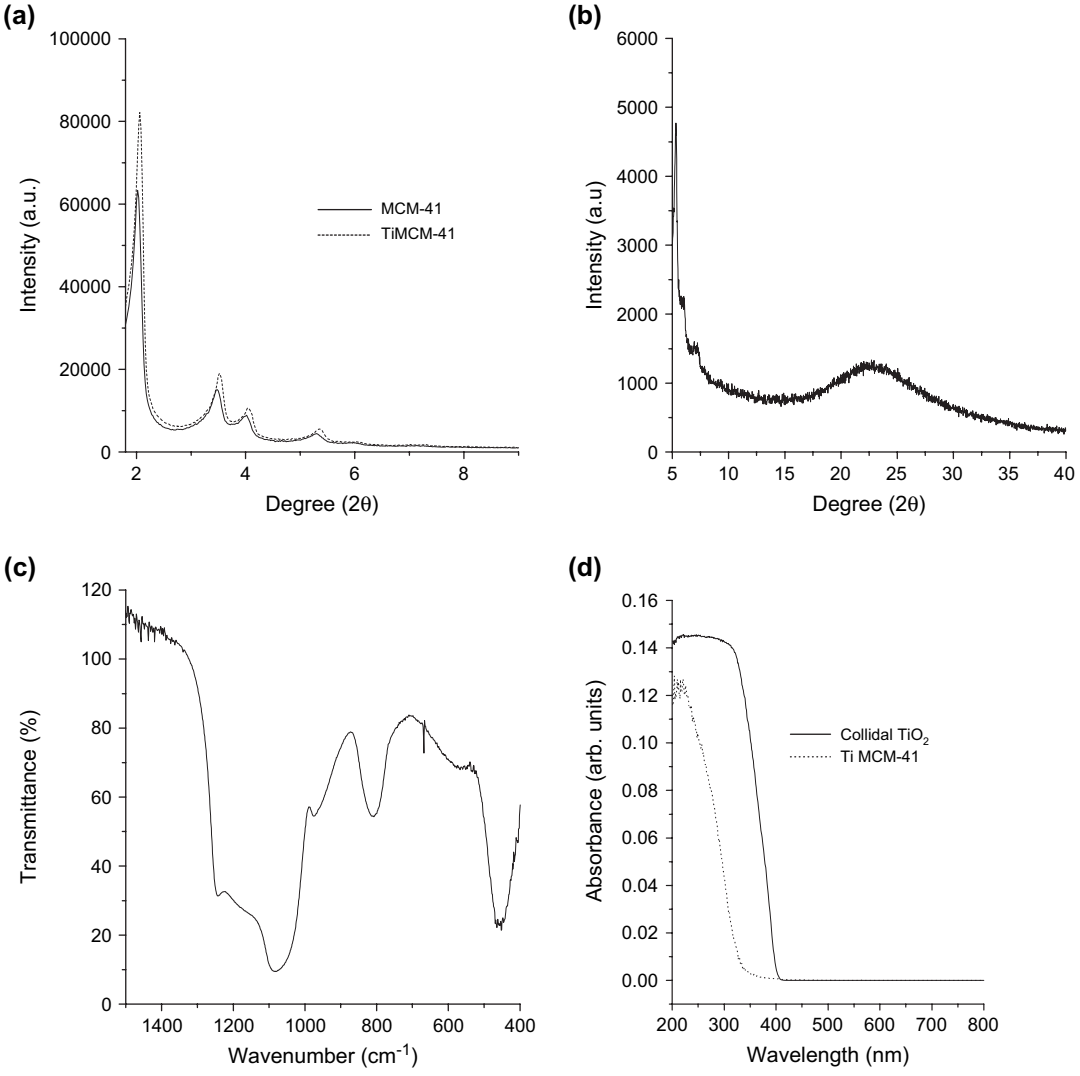

Fig. 1. (a) XRD spectra of calcined MCM-41 (—) and TiMCM-41 (···); (b) XRD spectrum of TiMCM-41 at higher 2θ; (c) FT-IR spectrum of TiMCM-41 and (d) solid state diffuse reflectance UV–vis spectra of colloidal TiO_2 (—) and TiMCM-41 (···).

catalyst surface by the photogenerated holes (h^+). Under ambient conditions, hydroxyl radicals can also arise from a series of reactions initiated by the scavenging of the photogenerated electrons (e^-).

$$TiO_2 \xrightarrow{h\nu} TiO_2(e^-_{CB}) + TiO_2(h^+_{VB}) \quad (1)$$

$$TiO_2(h^+_{VB}) + H_2O \rightarrow TiO_2 + OH^{\bullet} + H^+ \quad (2)$$

$$TiO_2(h^+_{VB}) + OH^- \rightarrow TiO_2 + OH^{\bullet} \quad (3)$$

$$TiO_2(e^-_{CB}) + OH^{\bullet} \rightarrow TiO_2 + OH^- \quad (4)$$

With PMS:

$$HOOSO_3^- + TiO_2(e^-_{CB}) \rightarrow SO_4^{\bullet -} + OH^- \quad (5)$$

$$HOOSO_3^- + TiO_2(e^-_{CB}) \rightarrow SO_4^{2-} + OH^{\bullet} \quad (6)$$

$$HOOSO_3^- + TiO_2(h^+_{VB}) \rightarrow SO_5^{\bullet -} + H^+ \quad (7)$$

$$2(SO_5^{\bullet -}) \xrightarrow{H_2O} 2HSO_4^- + O_2 \quad (8)$$

With PDS:

$$S_2O_8^{2-} + TiO_2(e^-_{CB}) \rightarrow SO_4^{2-} + SO_4^{\bullet -} \quad (9)$$

These reactions are of great importance in photodegradation processes. Unfortunately a significant part of electron–hole pairs recombine thus reducing the quantum yield. To avoid such electron–hole recombinations, we applied here electron acceptors such as peroxomonosulphate ($E^o = 1.84$ V) and peroxodisulphate ($E^o = 2.01$ V) to enhance the quantum yield in photodegradation of dyes using TiMCM-41 photocatalyst (refer reactions (5)–(9)).

3.2.1. Effect of PMS

To study the effect of PMS, experiments were carried out under natural pH in aqueous solution by following the

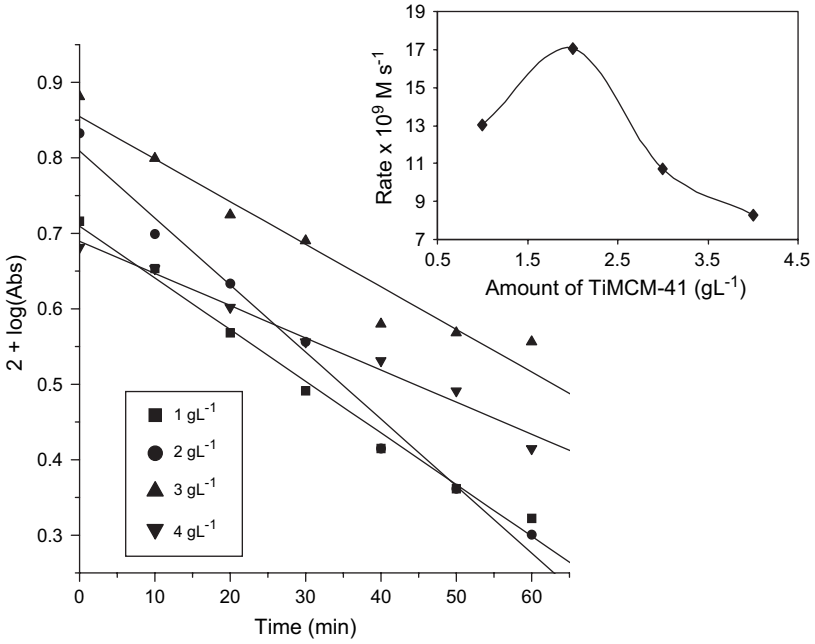

Fig. 2. Plot of variation of catalyst (TiMCM-41) upon irradiation time in the presence of fixed initial concentration of MeOr (5×10^{-5} M) and PMS (1.25×10^{-4} M). Inset shows plot of photodegradation rate for various amounts of TiMCM-41.

absorption maximum of MeOr ($\lambda_{max} = 466$ nm). First, the photodegradation process was evaluated with varying amount of the catalyst (TiMCM-41) at a fixed [MeOr] and [PMS] (5×10^{-5} M; 1.25×10^{-4} M). Fig. 2 shows the decrease of MeOr absorbance at different time intervals with respect to various catalyst amounts (1–4 g L^{-1}). The absorption of MeOr decreased reflecting the adsorption extent of MeOr on the TiMCM-41 surface. More the catalyst more will be the adsorption; hence the degradation rate is also more. Also by increasing the catalyst amount from a lower value, the amount of

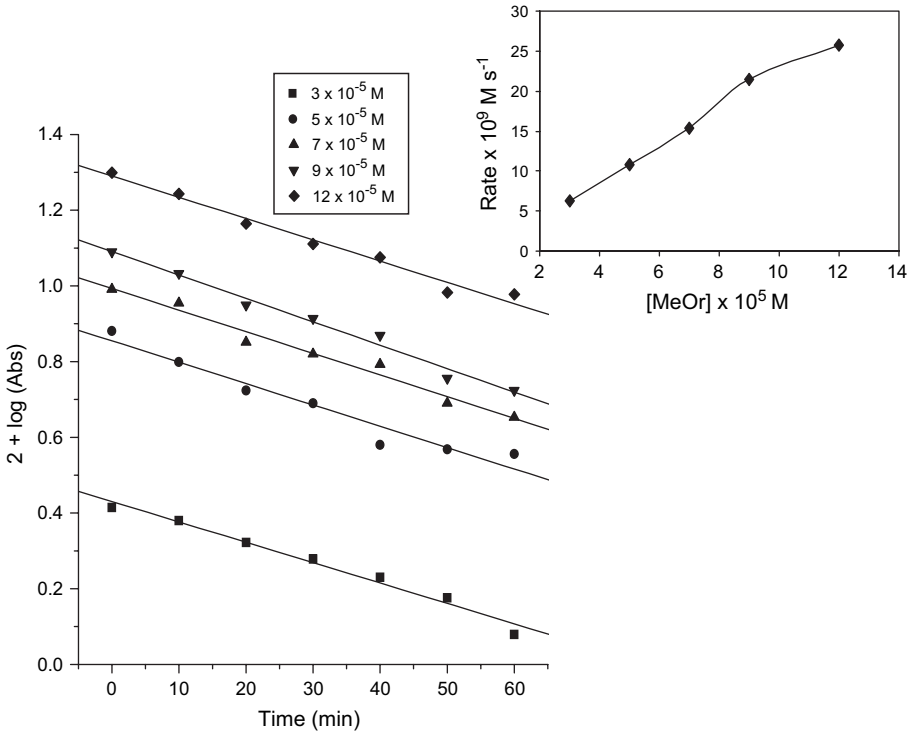

Fig. 3. Plot of variation of concentration of MeOr upon irradiation time in the presence of fixed amount of TiMCM-41 (3 g L^{-1}) and PMS (1.25×10^{-4} M). Inset shows plot of photodegradation rate for various concentrations of MeOr.

light absorbed by semiconductor particles increases and therefore the dye degradation also increases. The above reasons are necessary for the enhanced photodegradation process of MeOr with respect to TiMCM-41. But from the experiments it is concluded that optimum catalyst amount for maximum dye degradation is 2 g L^{-1}. Below or above this amount, there is decrease in the rate of dye degradation (see inset of Fig. 2). This is due to the fact that with increasing catalyst amount from a lower value, the amount of light absorbed by semiconductor particles increases and therefore the rate of dye degradation also increases. But eventually a point is reached at which the entire incident light is absorbed and the percentage can increase no further. For higher quantities of catalyst, a screening effect of excess particles occurs, which masks part of the photosensitive surface or reduces the penetration depth of the incident light. This may well increase the likelihood of losing scattered light to the exterior and in turn account for the reduction in the rate of dye degradation [27]. It is therefore clear from the figure that the photodegradation of MeOr occurs with time for each of the catalyst concentration. In a separate experiment, it was ensured that in the absence of photocatalyst (TiMCM-41), the photodegradation rate of MeOr was negligible. Similarly for unmodified MCM-41, no photodegradation rate was observed.

Secondly, at a fixed concentration of the TiMCM-41 (3 g L^{-1}) and [PMS] (1.25×10^{-4} M), the photodegradation was observed with the various initial concentrations of MeOr (Fig. 3). It was observed that the rate of dye degradation increased up to a particular concentration of [MeOr] (9×10^{-5} M), after which the degradation rate is comparatively less when compared to earlier lower concentrations of [MeOr] (see inset of Fig. 3). This can also be identified from the difference in rate values mentioned in Table 1. This may be due to saturation of adsorption of MeOr over the catalyst surface. To observe is there any change in the photodegradation rate, here we applied higher catalyst amount (3 g L^{-1}) for various initial concentrations of MeOr compared to the optimum catalyst amount (2 g L^{-1}) mentioned above. But the observed trend is almost same compared to the optimum catalyst amount used for the heterogeneous photocatalytic dye degradations.

Finally, photodegradation rates were observed for the variation of [PMS] at a fixed concentration of TiMCM-41 and MeOr (2 g L^{-1}; 5×10^{-5} M). It was observed that the rate increased with the increase in the [PMS], indicating the photodegradation of MeOr (Fig. 4). The increase in the photodegradation rate is due to the immediate trapping of the photogenerated electrons (e^-) by electron acceptors which in turn decreases the recombination of electron–hole pairs and thus enhances the optimum quantum yield.

Table 1
Evaluation of photodegradation rate for various initial concentrations of MeOr in the presence of fixed amount of TiMCM-41 (3 g L^{-1}) and PMS (1.25×10^{-4} M)

[MeOr] $\times 10^5$ M	3	5	7	9	12
Rate $\times 10^9$, M s^{-1}	6.219	10.745	15.316	21.411	25.788

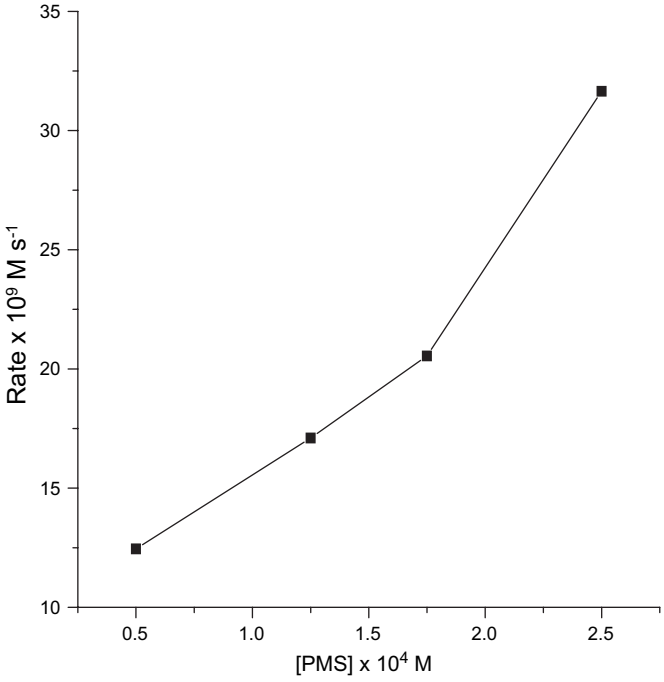

Fig. 4. Plot of photodegradation rate for various concentrations of PMS in the presence of fixed amount of TiMCM-41 (2 g L^{-1}) and MeOr (5×10^{-5} M).

3.2.2. Effect of PDS

To study the effect of PDS, experiments were carried out under natural pH by varying the amount of TiMCM-41 (1–4 g L^{-1}) by keeping constant concentration of [MeOr] and [PDS] (5×10^{-5} M; 1.25×10^{-3} M) (Fig. 5a). Similarly variation of [MeOr] and [PDS] were observed by keeping the other two substrates at fixed concentration (Fig. 5b and c). Altogether, the observed trend in results is almost same as the electron acceptor (PMS) but the photodegradation rate is quite low. The reason for such low reactivity is that the electron acceptor PMS may react with both $TiO_2(e^-_{CB})$ and $TiO_2(h^+_{VB})$ to generate active hydroxyl radicals whereas PDS may react only with $TiO_2(e^-_{CB})$ [28].

3.2.3. Effect of H_2O_2

In continuation of the above two electron acceptors, here we tried with another electron acceptor H_2O_2 thinking that we may get enhanced photocatalytic dye degradation but the observed trend is quite opposite, i.e., the system is inactive. The reason for such inactivity is H_2O_2 may function as a hydroxyl radical scavenger [29].

3.3. Comparison of photocatalytic efficiency

The observed rate of photocatalytic degradation with methyl orange in the presence of TiMCM-41 (0.020 Ti/Si ratio is approximately equivalent to colloidal TiO_2 of concentration 2.85×10^{-8} M ± 10%) without any electron acceptor is 1.344×10^{-9} M s^{-1} whereas with 1×10^{-5} M colloidal TiO_2 the observed rate is 2.495×10^{-9} M s^{-1} (Fig. 6). With PMS as electron acceptor the observed rate of degradation for the photocatalyst TiMCM-41 is about 1.708×10^{-8} M s^{-1}

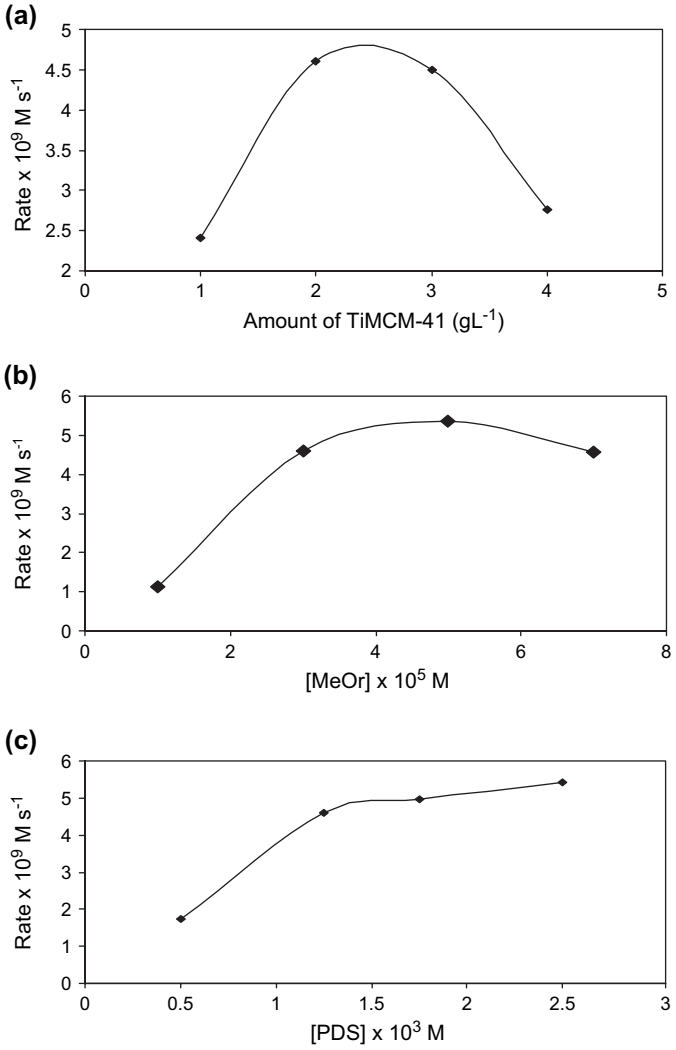

Fig. 5. (a) Plot of photodegradation rate for: (a) various amounts of TiMCM-41 in the presence of fixed concentration of MeOr (3×10^{-5} M) and PDS (1.25×10^{-3} M); (b) various concentrations of MeOr in the presence of fixed amount of TiMCM-41 (2 g L^{-1}) and PDS (1.25×10^{-3} M); (c) various concentrations of PDS in the presence of fixed amount of TiMCM-41 (2 g L^{-1}) and MeOr (3×10^{-5} M).

whereas in the case of colloidal TiO_2 the observed rate is 9.210×10^{-9} M s^{-1} at the same concentration of both catalyst and MeOr (Fig. 6). Similarly with PDS as electron acceptor the observed rate is 5.375×10^{-9} M s^{-1} for TiMCM-41 and 3.647×10^{-9} M s^{-1} for colloidal TiO_2. Thus, a 13-fold increase in the rate is observed for TiMCM-41 with PMS and a 4-fold increase in the rate with PDS which is quite higher compared to colloidal TiO_2 of about 4-fold with PMS and 2-fold with PDS. This is because modification of the semiconductor particle surface with MCM-41 nanopore materials would provide an effective environment for increasing the number of surface active sites for dye–semiconductor interaction which in turn increase the photodegradation processes. Thus the visible-light-induced dye degradation is based on the concept of light-induced charge injection from the excited dye to the semiconductor catalyst. Thus, the photoinduced interfacial electron transfer should take place in TiMCM-41,

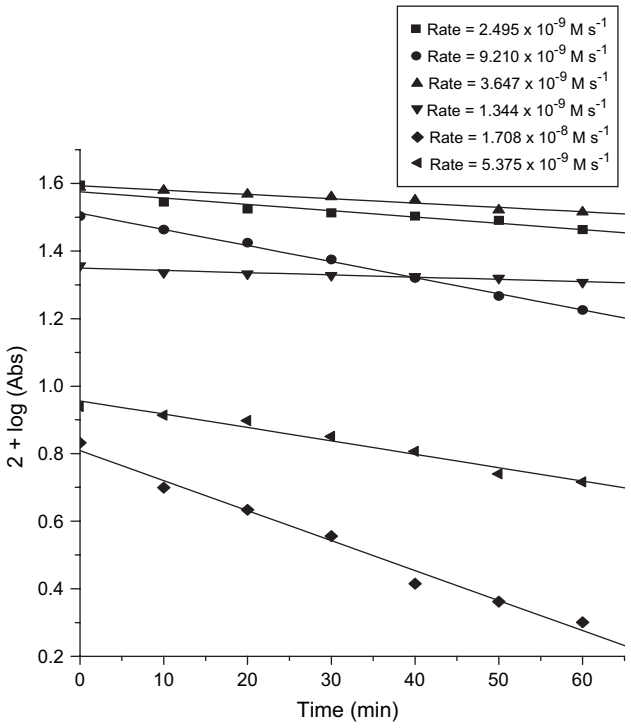

Fig. 6. Comparison of photodegradation rate of MeOr in the presence of: colloidal TiO_2 (■); colloidal TiO_2 with PMS (●); colloidal TiO_2 with PDS (▲); TiMCM-41 (▼); TiMCM-41 with PMS (◆); TiMCM-41 with PDS (◀). Concentrations are maintained as follows: MeOr (5×10^{-5} M); PMS (1.25×10^{-4} M); PDS (1.25×10^{-3} M), colloidal TiO_2 (1×10^{-5} M) and TiMCM-41 (2 g L^{-1}).

followed by the photodegradation of dye. Further characterization and identification of products formed by the utilization of MCM-41 nanopore materials for enhancing dye degradation of semiconductors is in progress and at present, we consider in this system also the possible degradation products is similar to the results published earlier with organic-capped anatase TiO_2 nanocrystals [30].

4. Mechanism

A feasible mechanism for the photocatalytic degradation of methyl orange is pointed out in the following figure.

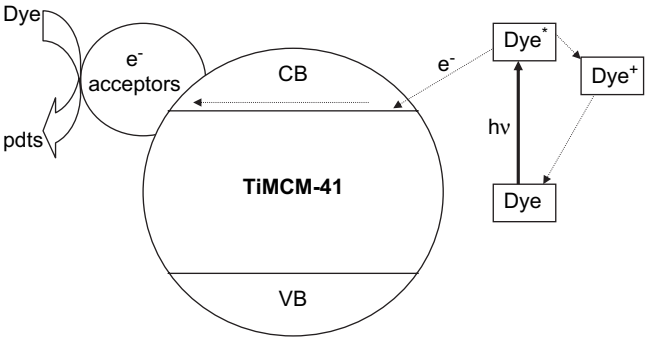

The various steps involved in the mechanism are as follows:

Light excitation of the dye is followed by electron transfer into the conduction band of the photocatalyst and is channeled/trapped by the electron acceptors to generate radicals,

which in turn effectively degrade the dye molecules to various products.

(i) Absorption of light:

$$\mathrm{Dye}_{(\mathrm{ads})} \xrightarrow{h\nu} {}^{*}\mathrm{Dye}_{(\mathrm{ads})} \quad (10)$$

(ii) Sensitization:

$${}^{*}\mathrm{Dye}_{(\mathrm{ads})} + \mathrm{TiO_2} \rightarrow \mathrm{Dye}^{+}_{(\mathrm{ads})} + \mathrm{TiO_2}(\mathrm{e}^{-}_{\mathrm{CB}}) \quad (11)$$

(iii) Trapping:

$$\text{Electron acceptors} + \mathrm{TiO_2}(\mathrm{e}^{-}_{\mathrm{CB}}) \rightarrow \mathrm{Ti^{IV}OH^{\bullet}} \quad (12)$$

(iv) Degradation:

$$\mathrm{Dye}_{(\mathrm{ads})} + \mathrm{Ti^{IV}OH^{\bullet}} \rightarrow \text{Products} \quad (13)$$

5. Conclusions

This study shows that nanometer sized titania supported MCM-41 nanopore materials is very active as a photocatalyst to effectively photodegrade methyl orange from solution in the presence of electron acceptors such as PMS and PDS. On comparison with colloidal TiO_2, TiMCM-41 shows 3 times higher photodegradation rate in the presence of PMS while 2 times higher in the case of PDS. The increase in the exposed catalyst surface area (TiMCM-41) is the reason for such performance improvement compared to colloidal TiO_2. Moreover, the improvement of these techniques for more exploitation of sun radiation could ensure more economic solutions to the problem of cleaning large volumes of waste water in short time.

Acknowledgement

The author, thank DST, New Delhi for the Fast Track Young Scientist award (SR/FTP/CS-13/2005). Also the author, thank the Director, National Institute of Technology, Trichy, for his keen interest and support for this work and also for providing a new lab under TEQIP programme.

References

[1] Ollis DF, Al-Ekabi H. Photocatalytic purification and treatment of water and air. Amsterdam: Elsevier; 1993.
[2] Serpone N, Pelizzetti E. Photocatalysis, fundamentals and applications. New York: Wiley; 1989.
[3] Schiavello M. Photocatalysis and environment. Dordecht: Kluwer; 1988.
[4] Preziosi P. Natural and anthropogenic environmental oestrogens: the scientific basis for risk assessment. Endocrine disrupters as environmental signalers: an introduction. Pure Appl Chem 1998;70:1617–31.
[5] Tyler CR, Routledge EJ. Oestrogenic effects in fish in English rivers with evidence of their causation. Pure Appl Chem 1998;70:1795–804.
[6] Muller S, Schlatter C. Estrogenic potency of nonylphenol in vivo – a case study to evaluate the relevance of human non-occupational exposure. Pure Appl Chem 1998;70:1847–53 and the references cited therein.
[7] Kresge CT, Leonowicz ME, Roth WJ, Vartuli JC, Beck JS. Ordered mesoporous molecular sieves synthesized by a liquid-crystal template mechanism. Nature 1992;359:710–2.
[8] Beck JS, Vartuli JC, Roth WJ, Leonowicz ME, Kresge CT, Schmitt KD, et al. A new family of mesoporous molecular sieves prepared with liquid crystal templates. J Am Chem Soc 1992;114:10834–43.
[9] Sayari A. Catalysis by crystalline mesoporous molecular sieves. Chem Mater 1996;8:1840–52.
[10] Corma A. From microporous to mesoporous molecular sieve materials and their use in catalysis. Chem Rev 1997;97:2373–420.
[11] Yanagisawa T, Shimizu T, Kuroda K, Kato C. The preparation of alkyltrimethylammonium–kanemite complexes and their conversion to microporous materials. Bull Chem Soc Jpn 1990;63:988–92.
[12] Zhao D, Huo Q, Feng J, Chmelka BF, Stucky GD. Nonionic triblock and star diblock copolymer and oligomeric surfactant syntheses of highly ordered, hydrothermally stable, mesoporous silica structures. J Am Chem Soc 1998;120:6024–36.
[13] Zhao D, Feng J, Huo Q, Melosh N, Fredrickson GH, Chmelka BF, et al. Triblock copolymer syntheses of mesoporous silica with periodic 50–300 angstrom pores. Science 1998;279:548–52.
[14] Anandan S, Yoon M. Photocatalytic activities of the nanosized TiO_2-supported Y-zeolites. J Photochem Photobiol C Photochem Rev 2003;4:5–18.
[15] Anandan S, Okazaki M. Dynamics, flow motion and nanopore effects of molecules present in the MCM-41 nanochannels – an overview. Microporous Mesoporous Mater 2005;87:77–92.
[16] Cheng M, Wang Z, Sakurai K, Kumata F, Saito T, Komatsu T, et al. Creation of acid sites on SBA-15 mesoporous silica by alumination. Chem Lett 1999;28:131–2.
[17] Luan Z, Maes EM, Van der Heide PAW, Zhao D, Czernuszewicz RS, Kevan L. Incorporation of titanium into mesoporous silica molecular sieve SBA-15. Chem Mater 1999;11:3680–6.
[18] Luan Z, Bae JY, Kevan L. Vanadosilicate mesoporous SBA-15 molecular sieves incorporated with *N*-alkylphenothiazines. Chem Mater 2000;12:3202–7.
[19] Zheng S, Gao L, Zhang QH, Guo JK. Synthesis, characterization and photocatalytic properties of titania-modified mesoporous silicate MCM-41. J Mater Chem 2000;10:723–7.
[20] Zheng S, Gao L, Zhang QH, Zhang WP, Guo JK. Preparation, characterization and photocatalytic properties of singly and doubly titania-modified mesoporous silicate MCM-41 by varying titanium precursors. J Mater Chem 2001;11:578–83.
[21] Bhattacharyya A, Kawi S, Ray MB. Photocatalytic degradation of orange II by TiO_2 catalysts supported on adsorbents. Catal Today 2004;98:431–9.
[22] Duonghong D, Borgarello E, Grätzel M. Dynamics of light-induced water cleavage in colloidal systems. J Am Chem Soc 1981;103:4685–90.
[23] Lin W, Han H, Frei H. CO_2 splitting by H_2O to CO and O_2 under UV light in TiMCM-41 silicate sieve. J Phys Chem B 2004;108:18269–73.
[24] Liqiang J, Xiaojun S, Weimin C, Zili X, Yaoguo D. The preparation and characterization of nanoparticle TiO_2/Ti films and their photocatalytic activity. J Phys Chem Solids 2003;64:615–23.
[25] Fenelonov VB, Romannikov VN, Yu Derevyankin A. Mesopore size and surface area calculations for hexagonal mesophases (types MCM-41, FSM-16, etc.) using low-angle XRD and adsorption data. Microporous Mesoporous Mater 1999;28:57–72.
[26] Henlein A. Small-particle research: physicochemical properties of extremely small colloidal metal and semiconductor particles. Chem Rev 1989;89:1861–73.
[27] Herrmann JM. Heterogeneous photocatalysis: fundamentals and applications to the removal of various types of aqueous pollutants. Catal Today 1999;53:115–29.
[28] Maruthamuthu P, Neta P. Radiolytic chain decomposition of peroxomonophosphoric and peroxomonosulfuric acids. J Phys Chem 1977;81:937–40.
[29] Fox MA, Dulay MT. Heterogeneous photocatalysis. Chem Rev 1993;93:341–57.
[30] Comparelli R, Fanizza E, Curri ML, Cozzoli PD, Mascolo G, Passino R, et al. Photocatalytic degradation of azo dyes by organic-capped anatase TiO_2 nanocrystals immobilized onto substrates. Appl Catal B Environ 2005;55:81–91.